Bio-Inspired Preparation of Fibrin-Boned Bionanocomposites of Biomacromolecules and Nanomaterials for Biosensing

Fangfang Han, Xin Qi, Lingyan Li, Lijuan Bu, Yingchun Fu Qingji Xie,* Manli Guo, Yanbin Li, Yibin Ying, and Shouzhuo Yao*

Learning from nature is one of the most promising ways to develop advanced functional materials. Here, inspired by blood coagulation, novel fibrin-boned bionanocomposites are reported as efficient immobilization matrices of biomacromolecules and nanomaterials for biosensing. Glucose oxidase (GOx), Au nanoparticles (AuNPs), and Fe_3O_4 magnetic nanoparticles (MNPs) are adopted as the model biomacromolecules and nanomaterials. By integrating the thrombin-triggered coagulation of fibrin with advanced surficial modification techniques, four kinds of immobilization strategies are developed and evaluated. Digital imaging, UV-vis spectroscopy, scanning/transmission electron microscopy, electrochemical methods, and N_2 adsorption-desorption isotherms are used to investigate the formation, immobilization efficiency, and performance of various bionanocomposites. The fibrin-boned networks show inherent biocompatibility, excellent adsorbability, porosity, and functionalization ability, endowing the bionanocomposites with high efficiencies in capturing AuNPs, MNPs and GOx (99%, 98%, and 57% captured under the given conditions, respectively), as well as significant mass-transfer and biocatalysis efficiencies. Therefore, the fibrin-boned bionanocomposites show great potential for biosensing, for example, a fibrin-AuNPs-GOx-glutaraldehyde bionanocomposites modified Au electrode is highly sensitive to glucose (145 μA cm^{-2} mM^{-1}) allowing for a limit of detection down to 25 nM, being much superior to those of the reported analogues. The presented experimental platform/strategy may find wide applications in the development of other bio/nano-materials/devices.

1. Introduction

Bionanocomposites that immobilize functional biomacromolecules and nanomaterials have shown great potential in various research fields including biosensing, biofuel cells, drug delivery, and so on, because they can combine individual properties with synergetic effects. The immobilization parameters and application performance are largely determined by the immobilization matrices/strategies. To date, besides the nanomaterials themselves acting as the matrices,[1] various artificial polymers, including polyaniline,[2] polydopamine,[3] and others,[4] as well as various natural biopolymers, mainly polysaccharides such as cellulose,[5] chitosan,[5c,5d,6] and alginate,[5c,5d,7] have been widely used to develop bionanocomposites for biomacromolecular immobilization. The biopolymers exhibit inherent biocompatibility, controllability, and degradability, and their bionanocomposites are thus receiving great attention in the areas of biosensing,[5d,6b,7] regenerative medicine,[5d] green materials,[8] and drug delivery.[5d] In comparison with polysaccharides, which have been widely utilized for bionanocomposite development and biosensing, it seems that other common biopolymers, proteins, nucleic acids, and lipids have been less frequently used for the same purpose, though they have different and/or even more abundant biofunctions. For example, streptavidin provides four sites to specifically bind biotin-modified biomacromolecules or other materials.[8] DNA scaffolds were designed to controllably immobilize two enzymes with given distances and orders through DNA hybridization linkage.[9] Lipid membranes were fabricated for horseradish peroxidase biosensors[10] and immobilization of antibodies to capture specific cells.[11] In our opinion, the development of functional and even intelligent bionanocomposites using biopolymers other than polysaccharides are of great importance.

Blood coagulation is one of the most ingenious, important, but complicated physiological actions in living systems. It includes a series of processes triggered by the initial bleeding to form fibrin-boned composites, which stop further bleeding. In this process, as briefly shown in **Scheme** 1 (path I), soluble

F. Han, X. Qi, L. Li, L. Bu, Dr. Y. Fu, Prof. Q. Xie, Prof. S. Yao
Key Laboratory of Chemical Biology and Traditional Chinese Medicine Research (Ministry of Education)
College of Chemistry and Chemical Engineering
Hunan Normal University
Changsha 410081, China
E-mail: ycfu@zju.edu.cn; xieqj@hunnu.edu.cn

Dr. Y. Fu, Prof. Y. Li, Prof. Y. Ying
College of Biosystems Engineering and Food Science
Zhejiang University
Hangzhou 310058, China

Dr. M. Guo, Prof. S. Yao
State Key Laboratory of Chemo/Biosensing and Chemometrics
College of Chemistry and Chemical Engineering
Hunan University
Changsha 410082, China

DOI: 10.1002/adfm.201400458

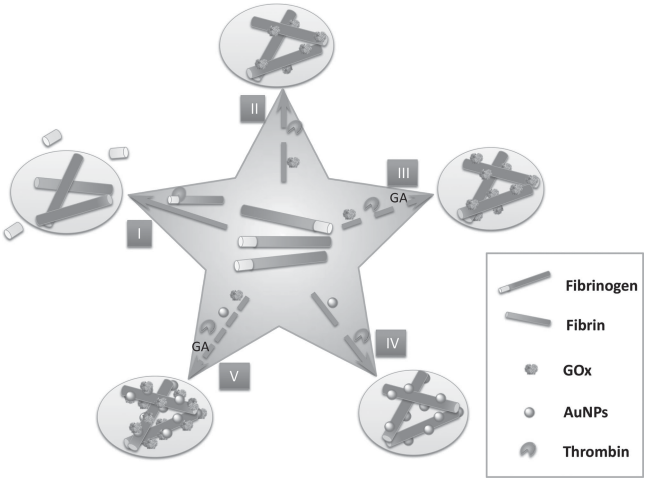

Scheme 1. Illustration of the fabrication of the fibrin-boned composites.

fibrinogen is cleaved by thrombin to yield insoluble fibrin which then coagulates to form networks.[12] This fibrin network can act as a scaffold to immobilize (entrap or absorb) lots of platelets and other species to form a firm film to block further bleeding. Unlike chemical polymerization, the blood coagulation is highly controlled by thrombin, which is intrinsically biocompatible and therefore highly interesting for biosensing applications. Thus, the surface and network properties of fibrin can be used to load the biosensing elements in a highly bioactive way. Fibrin has been used to load nanomaterials, enzymes, drugs, and even cells, to develop diversified fibrin composites in medical fields for tissue engineering,[13] drug delivery,[13c,14] and blood coagulation parameters estimation.[15] However, the development of fibrin-boned matrices for biosensing applications has rarely been investigated, most likely due to the fragility and significant porosity of fibrin films. The incorporation of nanoparticles may endow the fibrin-boned matrix with improved mechanical strength. Therefore, it is interesting and important to develop new functional fibrin-boned bionanocomposites with targets immobilized at high load/activity for biosensing applications. However, to the best of our knowledge, related research is rather limited.

Herein, inspired by the blood coagulation process, a fibrin scaffold is presented as an efficient immobilization matrix of biomacromolecules/nanomaterials to develop multifunctional bionanocomposites for biosensing. Glucose oxidase (GOx), Au nanoparticles (AuNPs), and Fe_3O_4 magnetic nanoparticles (MNPs) were utilized as the model biomacromolecules and nanomaterials, respectively. As briefly shown in Scheme 1, four kinds of immobilization strategies were developed, namely, physical immobilization of GOx (path II), both physical and chemical immobilization of GOx (glutaraldehyde (GA) covalent crosslinking) (path III), sole immobilization of single nanoparticles (AuNPs or MNPs, set AuNPs as example, path IV), and co-immobilization of nanoparticles (AuNPs and MNPs, set AuNPs as example) and GOx (path V). The properties of the biocomposites/bionanocomposites, including the load ratio of biomacromolecules/nanomaterials, mass transfer efficiency, biocatalysis performance, were examined. Digital imaging, UV-vis spectroscopy, scanning/transmission electron microscopy (SEM and TEM), electrochemical methods, and N_2 adsorption-desorption isotherm were used to investigate the preparation, characterization, and performance of the bionanocomposites. We found that the proposed fibrin-boned bionanocomposites showed great potential for the immobilization of GOx and nanomaterials for biosensing.

2. Results and Discussion

2.1. Fabrication and Characterization of the Fibrin-Boned Composites

UV-vis spectroscopy and digital imaging were utilized to monitor and characterize the immobilization of GOx and the nanoparticles on the fibrin matrix, as shown in **Figure 1**. To quantify the species of interest in the solution and the supernatant before and after the immobilization, respectively, the absorbance of fibrinogen[16] and GOx at 280 nm,[17] AuNPs at 520 nm,[18] and MNPs at 375 nm[19] were measured. After the addition of thrombin into the fibrinogen solution, the coagulation was immediately triggered. Dissolvable fibrinogen was cleaved into poorly dissolvable fibrin, which coagulated with each other in an end-to-end manner. This led to a decreasing fluidity of the solution (sample 1 of Figure 1A) and the appearance of a hydrogel-like white fibrin network within ca. 1 min. After around 20 min, a fibrin-boned compact hydrogel was obtained (sample 2 of Figure 1A). The UV-vis spectroscopic curve showed a peak of fibrinogen at 280 nm (curve 1 in Figure 1A), which drastically decreased after coagulation (curve 2 in Figure 1A). The residual absorption at 280 nm is ascribed to residual pieces of fibrinogen and some thrombin. When the coagulation occurred in the presence of GOx, similar results were obtained (samples 3 and 4, curves 3 and 4 of Figure 1A, before and after the immobilization, respectively). However, the final fibrin-GOx composites showed a light-yellow color, which might be due to the existence of yellow-colored GOx. The absorption curve after the coagulation still showed a distinctly higher peak at 280 nm than that without GOx (curve 4 in Figure 1A), which is due to the remainder of free GOx. When GA was used to covalently crosslink GOx and fibrin between their amino groups, a similar fibrin-GOx composite hydrogel was obtained (not shown). Although GA could also crosslink fibrin, a similar coagulation did not occur in the absence of thrombin, as shown in sample 5 of Figure 1A.

The same measurements were carried out in the presence of AuNPs, as shown in Figure 1B. We observed a clear and well dispersed solution in the absence (sample 1) and presence (sample 3) of GOx before the addition of thrombin. Surprisingly, after the addition of thrombin, the supernatants became very clear (samples 2 and 4), and the peak at 520 nm corresponding to the AuNPs in the supernatants disappeared (curves 2 and 4), indicating that nearly all of the added AuNPs were entrapped in the fibrin-boned bionanocomposites. Note that the concentration of the prepared AuNPs was fivefold of that prepared by the conventional Frens' method.[2a] Although the AuNPs became distinctly concentrated after the coagulation, the color of the coagulated AuNPs was still wine-red rather than blue or black, demonstrating that the AuNPs were well

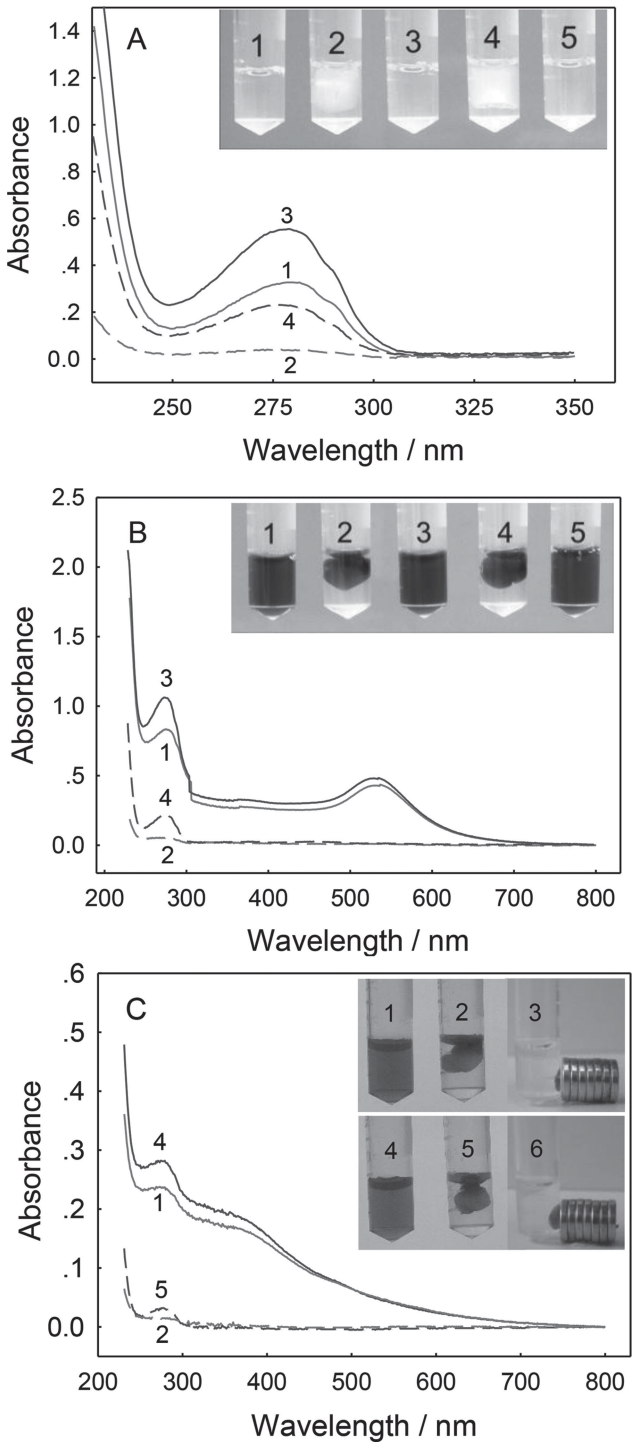

Figure 1. UV-vis spectra and digital camera pictures (inserts) of A) fibrinogen (1), fibrin (2), fibrinogen + GOx (3), fibrin-GOx (4), fibrinogen + GOx + GA (5); B) fibrinogen + AuNPs (1), fibrin-AuNPs (2), fibrinogen + AuNPs + GOx (3), fibrin-AuNPs-GOx (4), fibrinogen + AuNPs + GOx + GA (5); and C) fibrinogen + MNPs (1), fibrin-MNPs (2), fibrinogen + MNPs + GOx (4), fibrin-MNPs-GOx (5). Samples 3 and 6 in Figure 1C insert: the aggregation of samples 2 and 5 upon application of a magnetic field by a magnet, respectively. Concentrations: fibrinogen: 1 mg mL^{-1}, GOx: 1 mg mL^{-1}; thrombin: 77 nM; GA: 0.04% (v/v). The initial solution and supernatant of the fibrin-boned composites were threefold diluted before the measurements.

dispersed in the fibrin-boned bionanocomposites. The solution containing GA but no thrombin remained its good dispersion state (sample 5 of Figure 1B), proving again that GA could not trigger the coagulation without thrombin. Similar to the AuNPs, the MNPs were nearly all embedded after the coagulation, as demonstrated in Figure 1C. Additionally, the fibrin-MNPs bionanocomposites showed a strong and fast response to a magnet, as shown for samples 3 and 6, demonstrating the good magnetic properties of the immobilized MNPs. These results illustrate that the proposed fibrin-boned polymer is a very powerful matrix for the immobilization of nanoparticles, and the AuNPs or MNPs embedded in the fibrin-boned bionanocomposites can maintain their properties, which is very important for further applications.

To visualize the fibrin-boned composites, SEM (**Figure 2**) and TEM (**Figure 3**) images of the fibrin network (images A), the fibrin-GOx-GA biocomposites (images B), the fibrin-AuNPs-GOx-GA (images C), and the fibrin-MNPs-GOx-GA bionanocomposites (images D) were recorded. The fibrin presented a typical 3D fibrin network (images A).[12a] For the fibrin-GOx biocomposites, a similar 3D network was observed, except for the presence of lots of crumb-like particles on the surface, which might be GOx aggregates. For the fibrin-AuNPs-GOx-GA and the fibrin-MNPs-GOx-GA bionanocomposites, distinctly different structures were observed. Lots of AuNPs and MNPs were densely and uniformly dispersed on the fibrin bone, in good agreement with those in Figures 1B/C. Note that there were no nanoparticles in the area without fibrin matrix, demonstrating that the nanoparticles were located on the surface of fibrin but not dispersed in the fibrin container. Compared to the simple fibrin polymer, the nanoparticles-involved bionanocomposites presented a more porous structure. On the one hand, this implies that the present nanoparticles participated in coagulation of fibrin and then changed the final structure of the bionanocomposites, which should be noticed when the

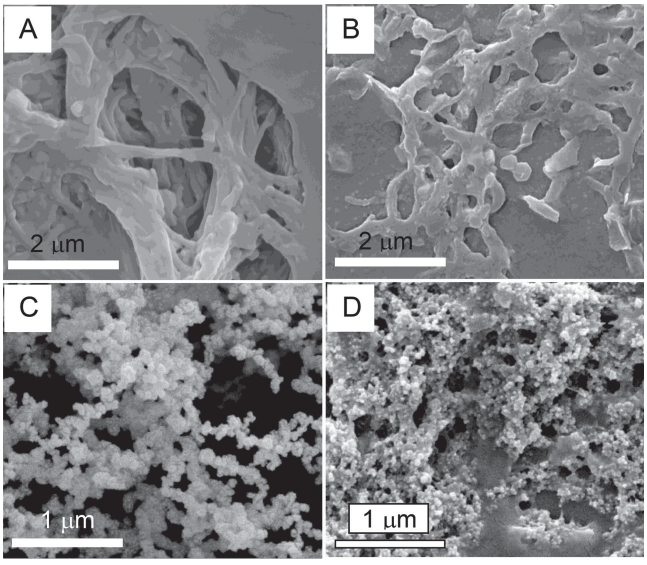

Figure 2. SEM images of fibrin (A), fibrin-GOx-GA (B), fibrin-AuNPs-GOx-GA (C), and fibrin-MNPs-GOx-GA (D).

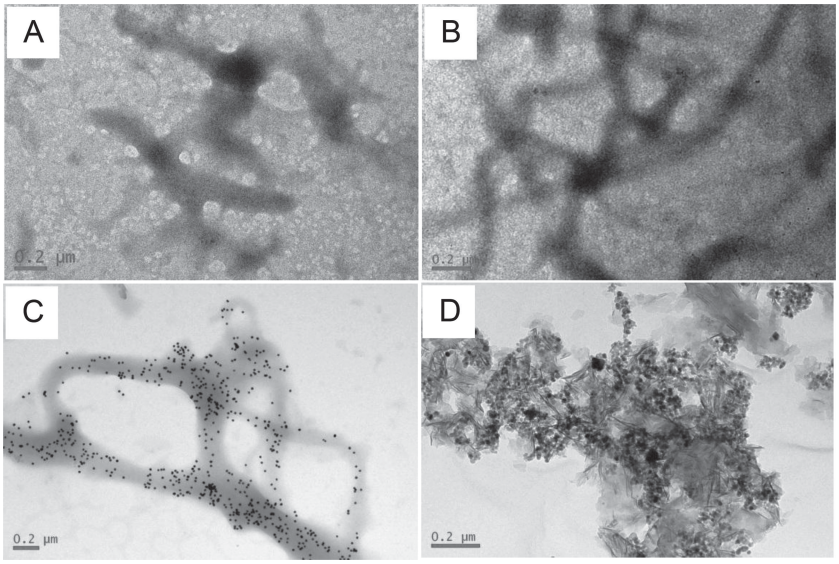

Figure 3. TEM images of fibrin (A), fibrin-GOx-GA (B), fibrin-AuNPs-GOx-GA (C), and fibrin-MNPs-GOx-GA (D).

nanoparticles are used for therapy in vivo due to the interruption of blood coagulation. On the other hand, the enhanced porosity should greatly increase the surface area and mass transfer efficiency of/in the bionanocomposites, and therefore be beneficial for further applications. Furthermore, the incorporation of nanoparticles in the bionanocomposites should also enhance the mechanical strength to promote the stability.[3b] These results proved again the significant immobilization capability of fibrin-boned matrices due to its inherent porous structure and high adsorbability, as well as their promising potential for applications.

N_2 adsorption-desorption isotherms and pore-size distributions of fibrin and its composites are shown in Figure S1 (Supporting Information), and bovine serum albumin (BSA) aggregates were used for comparison. For fibrin, fibrin-GOx-GA, and fibrin-AuNPs-GOx-GA (as an example of the nanoparticles-involved composites), the Brunauer–Emmet–Teller (BET) surface areas were estimated to be 40, 38, and 52 $m^2\ g^{-1}$, respectively. All the BET surface areas are obviously larger than that of BSA (6 $m^2\ g^{-1}$) and that of egg albumin (5–21 $m^2\ g^{-1}$).[20] The BET surface area of the fibrin-AuNPs-GOx-GA is even comparable with that of multiwalled carbon nanotubes (60 $m^2\ g^{-1}$).[21] The above data demonstrate that the organized fibrin network exhibits a higher surface area than that of protein aggregates, and the incorporation of nanoparticles promotes the porosity. The isotherm could be classified as a type-IV isotherm, indicating the presence of textural mesopores, as also proven in the pore-size distribution curves. The average pore diameters according to the Bopp-Jancso-Heinzinger (BJH) method are 11.03 nm (fibrin-AuNPs-GOx-GA), 20.54 nm (fibrin-GOx-GA), and 12.58 nm (fibrin), respectively. The mesopores might be formed by fibrin networks and nanoparticles. Large pores as those observed in the SEM and TEM images were not obtained, which might be related to a collapse during the sample preparation.

2.2. Immobilization Efficiency of Nanoparticles and GOx in Fibrin-Boned Composites

The fibrin-boned matrices have shown a significant immobilization capability of biomacromolecules and nanomaterials. The load ratios of nanoparticles and GOx were also evaluated. For the nanoparticles (AuNPs and MNPs), the load ratios were investigated using UV-vis spectroscopy, as shown in Figure 1. The absorption peaks of the AuNPs at 520 nm and the MNPs at 375 nm were selected for the quantification in the solution and the supernatant before and after the immobilization, respectively (as listed in Table S1, Supporting Information). Subtraction of the residual absorbance from the initial one gives the loaded one. The absorbance of the AuNPs in the supernatants of fibrin-AuNPs and fibrin-AuNPs-GOx composites decreased to 0.006 ± 0.006 (n = 3, n is the number of parallel experiments, the same as below) and 0.005 ± 0.005, respectively, being 1% of that of the initial absorbance (0.434 ± 0.003 and 0.45 ± 0.04, respectively). We calculated the load ratios to be both 99%. The absorbance of the MNPs (at 375 nm) in the supernatants of the fibrin-MNPs (0.003 ± 0.002) and fibrin-MNPs-GOx (0.003 ± 0.001) bionanocomposites was also very small, in comparison with those of the initial reactant solutions (0.17 ± 0.01 and 0.185 ± 0.004, respectively). We calculated the load ratios of MNPs to be both 98%. These results prove that the proposed fibrin-boned matrix could capture nearly all the added nanoparticles. Therefore, the fibrin-boned polymer presents an almost perfect matrix for capturing these nanoparticles and a very promising candidate to design various bionanocomposites for diversified applications.

The load ratios of GOx in different fibrin-boned composites were indirectly obtained by quantifying the initial and residual amount of GOx in the supernatant through detecting the kinetics of enzymatic catalysis by UV–vis spectroscopy. Four fibrin-boned composites, including fibrin-GOx (solely physical adsorption), fibrin-GOx-GA (physical adsorption and chemical crosslinking), fibrin-AuNPs-GOx-GA (co-immobilization of AuNPs and GOx), and fibrin-MNPs-GOx-GA (co-immobilization of MNPs and GOx) were investigated and compared, as shown in **Figure 4**. The measurement principle is as follows:[22] In the reaction mixture of the phosphate buffer solution (PBS) containing *o*-dianisidine dihydrochloride, glucose, and horseradish peroxidase (HRP), the solution-state GOx (native) or the immobilized GOx catalyzes the oxidation of glucose and produces H_2O_2. Then the coexisting *o*-dianisidine dihydrochloride is oxidized to yield a brown product in the presence of solution HRP. Therefore, the increase rate of the absorbance can be used to quantify the amount of GOx (assuming the activity of the native and the immobilized GOx is identical), then the load ratios of GOx in the fibrin-boned composites could be indirectly measured via the subtraction of the residual absorbance change at 436 nm in 180 s from the initial one (as listed in **Table 1**). The absorbance changes at 436 nm in 180 s in the supernatants of

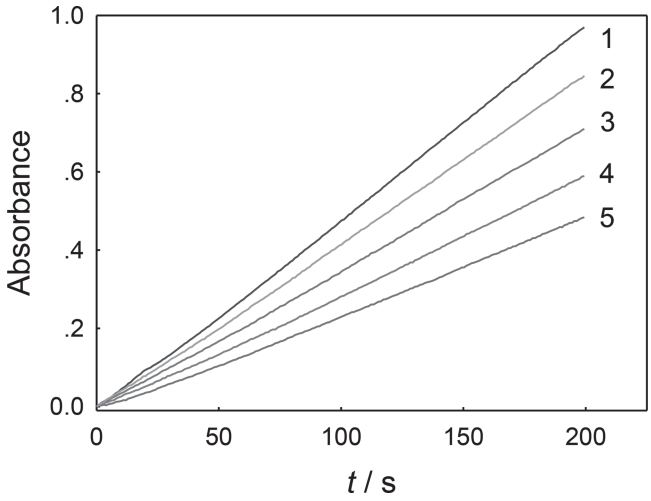

Figure 4. Real-time monitoring of enzymatic catalysis kinetics by UV–vis spectroscopy of the addition of 0.010 mL of a mixture of 0.17 mg mL^{-1} GOx and 1 mg mL^{-1} fibrinogen (1) and the supernatant of fibrin-GOx (2), fibrin-GOx-GA (3), fibrin-MNPs-GOx-GA (4) and fibrin-AuNPs-GOx-GA (5), into another reaction mixture (2.5 mL of 0.25 mM *o*-dianisidine dihydrochloride in PBS **1** buffer + 0.50 mL of 0.50 M glucose + 0.010 mL of 1.4 mg mL^{-1} HRP). Concentrations: fibrinogen: 1 mg mL^{-1}, GOx: 0.17 mg mL^{-1}; thrombin: 77 nM; GA: 0.04% (v/v). The absorbance was measured at 436 nm.

fibrin-GOx, fibrin-GOx-GA, fibrin-MNPs-GOx-GA, and fibrin-AuNPs-GOx-GA were 0.76 ± 0.01, 0.65 ± 0.02, 0.54 ± 0.01, and 0.37 ± 0.02, being 87%, 75%, 62%, and 43% of that in the GOx solution (0.87 ± 0.01), giving load ratios of 13%, 25%, 38%, and 57%, respectively. Here, the fibrin-boned polymer provided multi-surface properties for immobilization, leading to a significant increase of the GOx load ratio integrating both chemical and physical methods rather than the sole physical one. On the other hand, the fibrin-boned polymer acted as a perfect matrix for nanoparticles, thus bionanocomposites of much higher surficial area and nanoparticles sites can be obtained showing high adsorbability for other species such as GOx, as shown here. The above results have highlighted the significant load capability of fibrin and demonstrated its potential as new and efficient immobilization matrices of biomacromolecules.

2.3. Mass Transfer Efficiency in the Fibrin-Boned Composites

Mass transfer efficiency is another key factor for the evaluation of the immobilization matrix, because it is an important reflection of the structure, and it affects the adsorption process and catalysis/biocatalysis applications through controlling the diffusion of the substrates/products. Here, an electrochemical method was used. The bionanocomposites were transferred onto Au electrodes, then the mass transfer efficiencies were characterized and compared by detecting the oxidation current of H_2O_2 (with identical bulk concentrations) on relevant electrodes at 0.7 V. A bare Au electrode was used as the control. Note that because of the strong magnetism of the fibrin-MNPs-GOx bionanocomposites, these bionanocomposites were readily transferred onto the Au electrodes by simply applying a magnet, which showed one of the promising applications of the fibrin-boned multifunctional materials. The steady-state current responses are shown in **Figure 5**. We obtained current responses of 14 ± 1, 11 ± 1.3 and 8 ± 0.4 μA (n = 3, same as below) on the fibrin-AuNPs-GOx-GA, fibrin-MNPs-GOx-GA, and fibrin-GOx-GA modified Au electrodes, respectively, being as high as 52%, 41% and 30% of that on the bare electrode (27 ± 0.4 μA), respectively. These results are much better than that of conventional polymer films of 2,5-dimercapto-1,3,4-thiadiazole (DMcT) prepared chemically (26%) or electrochemically (8.6%), and are close to that of highly porous metal-organic polymer films of Au-DMcT (65%) or Pt-DMcT (58%), as reported in our previous work.[23] Here, the impressive mass-transfer efficiency of the fibrin-boned composites is most likely ascribed to the inherent high porosity of the fibrin network, which should be notably beneficial for enzyme catalysis. Moreover, the fibrin-AuNPs-GOx-GA and fibrin-MNPs-GOx-GA bionanocomposites show much higher mass transfer efficiencies than the fibrin-GOx-GA, and this may be attributed to the more porous structure caused by the high adsorbability of the fibrin to the nanoparticles, as discussed above. Compared with the fibrin-MNPs-GOx/Au electrode, a larger current response at the fibrin-AuNPs-GOx/Au electrode was observed, being attributed to the higher GOx load as well as the enhanced conductivity and mass transfer efficiency for AuNPs as compared to MNPs. Note that the nanoparticles in the film might chemically decompose

Table 1. Biocatalysis performance of various modified electrodes to glucose (r^2 values for LDR are all >0.99).

Modified electrode	sensitivity [μA cm^{-2} mM^{-1}]	LDR [μM]	LOD [nM]
fibrin-GOx/Au	35	1–3555	245
fibrin-GOx-GA/Au	93	1–1555	68
fibrin-MNPs-GOx-GA/Au	126	1–1555	36
fibrin-AuNPs-GOx-GA/Au	145	1–1555	25

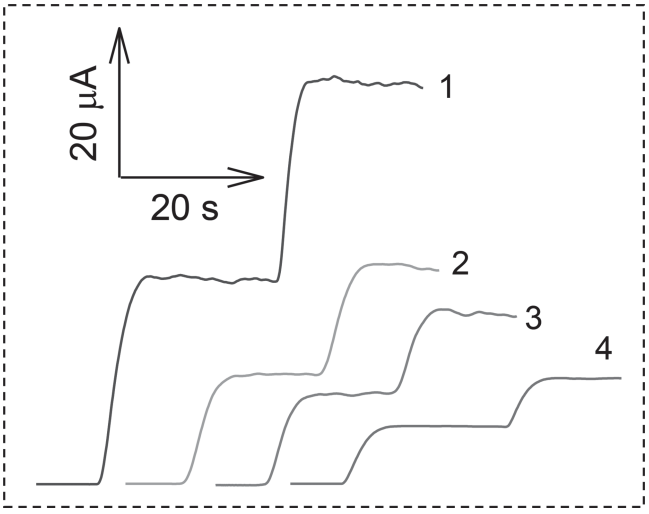

Figure 5. Chronoamperometric responses on bare Au (1), fibrin-AuNPs-GOx-GA/Au (2), fibrin-MNPs-GOx-GA/Au (3), and fibrin-GOx-GA/Au (4) electrodes at 0.7 V in pH 7.0 PBS **1** to incremental additions of 1 mM H_2O_2.

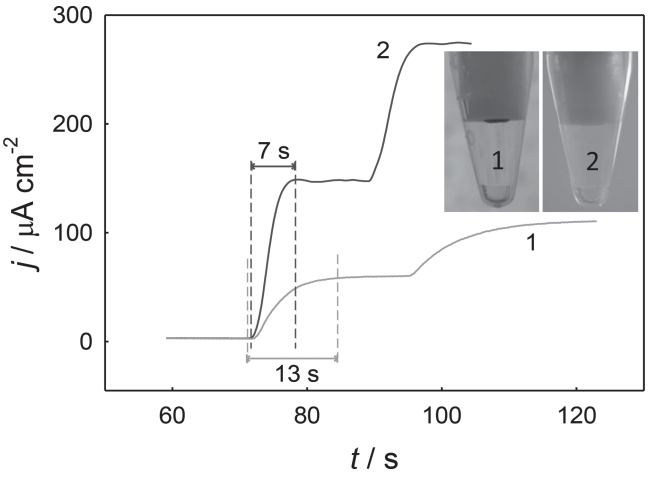

Figure 6. Chronoamperometric responses on fibrin-AuNPs-GOx/Au (1) and fibrin-AuNPs-GOx-GA/Au (2) electrodes at 0.7 V in pH 7.0 PBS **1** to incremental additions of 1 mM glucose.

H_2O_2 during the detection, which may disturb the estimation of the mass transfer efficiency. Here, the influence of the nanoparticles in the fibrin film on the estimation of the mass transfer efficiency using H_2O_2 as probe was examined. H_2O_2 was mixed with AuNPs colloids or MNPs suspensions, the concentrations of H_2O_2 before and after a 5-min mixing were estimated and compared by the potentiostatic method at 0.7 V on an Au electrode. H_2O_2 solutions of identical concentration were used as the control. As shown in Figure S2 (Supporting Information), the successive addition of H_2O_2 solution, mixtures of H_2O_2 and AuNPs or MNPs gave the same responses immediately after the mixing, indicating that the concentration of H_2O_2 showed few changes at this time point. After 5 min, the responses were identical to each injection and those before 5 min. Therefore, the influence of nanoparticles on the concentration of H_2O_2 during the mass transfer measurement (generally less than 1 min) should be negligible in this case.

Cyclic voltammetry (CV) and electrochemical impedance spectroscopy (EIS) experiments using $K_3Fe(CN)_6/K_4Fe(CN)_6$ revealed similar results, as shown in Figure S3, Supporting Information. Au electrodes modified by fibrin-GOx, fibrin-GOx-GA, fibrin-MNPs-GOx-GA, and fibrin-AuNPs-GOx-GA were studied. As shown in Figure S3, Supporting Information, when GA was used, the charge transfer resistances of nanoparticles-containing composites films (fibrin-AuNPs-GOx-GA (curve 3) and fibrin-MNPs-GOx-GA (curve 4)) were lower than that of films without nanoparticles, and this could be attributed to the enhanced porosity and conductivity caused by the nanoparticles. When GA was absent, the fibrin-GOx film (curve 2) showed the lowest charge transfer resistance of the fibrin composites, which might be due to its loose structure, as also proven in **Figure 6**. The CV results agreed with EIS.

The important role of GA on the immobilization efficiency and on the structure of the bionanocomposites was also investigated. Although GA could not cause the coagulation, it increased the GOx load ratio by the covalent crosslinking, as mentioned above. Interestingly, we observed that the fibrin-boned bionanocomposites with GA presented much thinner (compact) films on the Au electrodes than those without GA, as shown in Figure 6 for fibrin-AuNPs-GOx films without (sample 1) or with (sample 2) GA. Note that other parameters were similar except for the addition of GA during the coagulation. Therefore, potentiostatic responses of the fibrin-AuNPs-GOx/Au and fibrin-AuNPs-GOx-GA/Au electrodes were examined and compared to investigate the difference. The fibrin-AuNPs-GOx-GA/Au showed a much higher response (146 μA cm^{-2}, curve 2) than the fibrin-AuNPs-GOx/Au (57 μA cm^{-2}, curve 1), as well as a distinctly faster response time of 7 s over 13 s, respectively. Here, besides increasing the immobilization ratio of GOx, the proposed fibrin matrix allowed to produce appropriately more compact films of bionanocomposites through crosslinking between fibrin fibriners. Such thinner and more compact films should greatly decrease the mass transfer distance and accelerate the response. Furthermore, this result may inspire us to regulate the structure and performance of the fibrin-boned bionanocomposites via controlling the GA crosslinking in the fibrin matrix. This may be one of the next steps to develop and improve the fibrin-boned matrix.

2.4. The Biocatalysis Performance of the Fibrin-Boned Composites

The biocatalysis efficiencies of various fibrin-boned composites were examined. Four composites-modified electrodes were fabricated as described above under optimized conditions (as listed in Table S2, Supporting Information), including the fibrin-GOx, fibrin-GOx-GA, fibrin-MNPs-GOx-GA, and fibrin-AuNPs-GOx-GA. The amperometric responses to glucose and the calibration curves are shown in **Figure 7**, and the values of biocatalysis sensitivity (*S*), linear detection range (LDR), and limit of detection (LOD) are listed in Table 1. The sensitivities of the fibrin-GOx, fibrin-GOx-GA, fibrin-MNPs-GOx-GA, and fibrin-AuNPs-GOx-GA modified electrodes were 35 μA cm^{-2} mM^{-1}, 93 μA cm^{-2} mM^{-1}, 126 μA cm^{-2} mM^{-1}, and 145 μA cm^{-2} mM^{-1}, respectively. Note that the sensitivities of the fibrin-GOx-GA, fibrin-MNPs-GOx-GA, and fibrin-AuNPs-GOx-GA modified electrodes are much better than that of the reported analogues, which were generally lower than 20 (mostly <10) μA cm^{-2} mM^{-1}.[24] In addition, the LOD is two orders of magnitude lower than that of the reported analogues.[24b,25] This excellent performance mainly results from the various advantages of the fibrin-boned bionanocomposites: (1) The fibrin-boned network provides abundant sites for the direct immobilization of GOx in physical and chemical ways. It also enables an ultrahigh adsorbability of nanoparticles, which act further as valuable sites for the immobilization of GOx and the reservation of biocatalysis activity. (2) The fibrin-boned composites with significant porosity greatly facilitate the mass transfer of the substrates and products and thus promote the enzyme catalysis efficiency. (3) Fibrin itself and fibrin composites are highly biocompatible and allow GOx to retain activity. Therefore, the high biocatalysis efficiency should prove the promising application potential of the proposed fibrin-boned matrix.

The stability of fibrin-boned composites was also examined by daily detection of the catalysis performance. As shown in Figure S4, Supporting Information, the current response of the

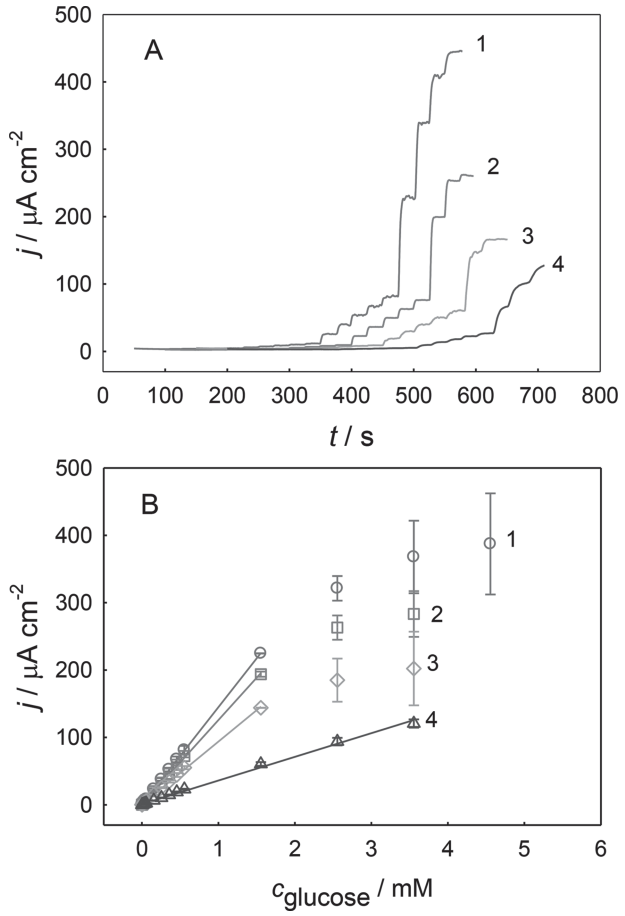

Figure 7. Chronoamperometric responses to successive additions of glucose (A), and the calibration curves (B) obtained in PBS **1** (pH 7.0) at 0.7 V vs. SCE for fibrin-AuNPs-GOx-GA (1), fibrin-MNPs-GOx-GA (2), fibrin-GOx-GA (3), and fibrin-GOx (4) modified Au electrodes.

fibrin-MNPs-GOx-GA, fibrin-AuNPs-GOx-GA, and fibrin-GOx-GA modified Au electrodes maintained 83%, 80% and 76% of the initial responses after 12 days, respectively. This proves that the proposed immobilization method and matrices provide satisfactory stability. The stability of fibrin-GOx was also examined by the same method, but the current response decreased seriously in several days (data not shown), which might be due to the gradual falling-off of the loose fibrin-GOx film without the reinforcement by nanomaterials and GA.

3. Conclusions

In summary, inspired by blood coagulation, we have successfully exploited fibrin-boned bionanocomposites as new and efficient immobilization matrices of biomacromolecules/nanomaterials for biosensing applications. The fibrin-boned matrix presented diversified surficial properties, highly porosity, biocompatibility, controllability, functionability, showing great potential in the immobilization of GOx and nanomaterials to prepare multifunctional bionanocomposites. The proposed fibrin-boned bionanocomposites possessed an impressive immobilization ratio of GOx and nanoparticles (close to 100% for AuNPs or MNPs), as well as strongly enhanced mass transfer efficiencies and significant biocatalysis performance. All the results presented here provide new insights into fibrin-boned matrices that can be widely used as an efficient immobilization platform for biomacromolecules/nanomaterials. The new materials/strategy may provide promising pathways to develop bio/nanodevices for various fields.

4. Experimental Section

Instrumentation and Reagents: All electrochemical experiments were conducted on a CHI660C electrochemical workstation (CH Instruments Inc., Austin, TX), and a conventional three-electrode electrolytic cell was used. Au disk electrodes with 2.0 mm diameter (0.031 cm^2 area) served as the working electrode, a KCl-saturated calomel electrode (SCE) served as the reference electrode, and a carbon rod served as the counter electrode. All potentials are taken with respect to SCE. TEM images were collected on a JEM-2100F transmission electron microscope (Japan). SEM images were collected on a JEM-6700F field emission scanning electron microscope. Nitrogen adsorption–desorption measurements were performed on a Micromeritics TriStar surface area and porosity analyzer (Micromeritics Instrument Corporation, USA). The UV-vis spectra were recorded on a UV-2450 UV-vis spectrophotometer (Shimadzu, Japan).

GOx (EC 1.1.3.4; type II from *Aspergillus niger*, ≈150 kU g^{-1}), fibrinogen, and thrombin from human serum plasma were purchased from Sigma. Glucose was obtained from Shanghai Chemicals Station. Au nanoparticles (AuNPs) were prepared according to a typical protocol described in the literature,[26] while Fe_3O_4 magnetic nanoparticles (MNPs) were purchased from Henan Huier Nano Technology CO., LTD. Note that the concentration of the prepared AuNPs is fivefold of that prepared by the conventional Frens' method. Two different pH 7.0 phosphate buffer solutions (PBS) were used: PBS **1** (0.10 M KH_2PO_4-K_2HPO_4 + 0.10 M K_2SO_4) for chemical and electrochemical reactions and PBS **2** (0.010 M NaH_2PO_4-Na_2HPO_4 + 0.15 M NaCl) for biochemical reaction processes. All other chemicals were of analytical grade or of better quality and used as received. All experiments were performed at room temperature using Milli-Q ultrapure water (Millipore, ≥ 18 MΩ cm).

Preparation of Fibrin-Boned Composites: The fibrin-boned composites were prepared as follows: 1.0 mg mL^{-1} fibrinogen, or/and 1.0 mg mL^{-1} GOx, or/and AuNPs (or MNPs) were dissolved in 0.6 mL pH 7.0 PBS **2**, and then 0.05 mL 1 μM thrombin was added to trigger coagulation, transferring soluble fibrinogen into a three-dimensional network of insoluble fibrin, and large amounts of GOx, or/and AuNPs (or MNPs) were entrapped in situ into the fibrin-boned composites. For comparison, 1.0 mg mL^{-1} fibrinogen, 1.0 mg mL^{-1} GOx, or/and AuNPs were dissolved in 0.6 mL pH 7.0 PBS **2**, then 0.05 mL 0.5% glutaraldehyde (GA) solution were added to trigger the crosslinking reaction.

The bare Au electrodes were rinsed thoroughly according to a reported protocol with minor modifications[27] and was immediately used for modifying composites. The construction of the enzyme films was as follows: 3 μL of PBS **2** (0.1 mL) containing 1.0 mg mL^{-1} fibrinogen, 6.7 mg mL^{-1} GOx, or/and AuNPs (or MNPs) was drop-cast on the Au electrode. Then, 1 μL 0.4 μM thrombin or/and 1 μL 0.5% GA solution was drop-cast on the modified Au electrode to trigger the crosslinking reaction, as well as to entrap GOx or/and AuNPs (or MNPs), yielding fibrin-GOx, fibrin-GOx-GA, fibrin-MNPs-GOx-GA, and fibrin-AuNPs-GOx-GA/Au electrodes, respectively, and they were dried at room temperature. When not in use, the prepared GOx electrodes were stored in pH 7.0 PBS **1** at 4 °C (refrigerator).

Bare Au electrodes were characterized in PBS **1** containing 1.0 mM $K_4Fe(CN)_6$ and 1.0 mM $K_3Fe(CN)_6$ by cyclic voltammetry (at 100 mV s^{-1}) and electrochemical impedance spectroscopy (EIS), which were generally performed after each modification for comparisons among and

better understanding of various surfaces. For the EIS measurements, the working electrode potential was fixed at the formal potential of the $Fe(CN)_6^{3-/4-}$ couple after being conditioned at this potential for 100 s.

Amperometric Measurements. Measurements of the prepared enzyme electrodes were carried out under solution-stirred conditions in pH 7.0 PBS **1**, and the response current was marked with the change value between the steady-state current after addition of a substrate and the initial background current without the substrate.

Supporting Information

Supporting Information is available from the Wiley Online Library or from the author.

Acknowledgements

This work was supported by the National Natural Science Foundation of China (Grants 21075036, 21175042, 21105026), the Foundation of Hunan Province (Grant 11JJ4014), Specialized Research Fund for the Doctoral Program of Higher Education (20114306120004), Program for Science and Technology Innovative Research Team in Higher Educational Institutions of Hunan Province and State Key Laboratories of Chemo/Biosensing and Chemometrics (Grant 201104), and the Fundamental Research Funds for the Central Universities. The authors thank Prof. Mancai Xu, Prof. Xianglin Xie, Mr. Jiang Liu and Dr. Wenli Zhou in Hunan Normal University for the help on N_2 adsorption-desorption measurements and analysis.

Received: February 10, 2014
Revised: April 1, 2014
Published online: May 26, 2014

[1] a) Z. Wen, S. Ci, J. Li, *J. Phys. Chem. C* **2009**, *113*, 13482; b) B.-Y. Hua, J. Wang, K. Wang, X. Li, X.-J. Zhu, X.-H. Xia, *Chem. Commun.* **2012**, *48*, 2316.

[2] a) Y. G. Liu, X. M. Feng, J. M. Shen, J. J. Zhu, W. H. Hou, *J. Phys. Chem. B* **2008**, *112*, 9237; b) Z. Liu, J. Wang, D. Xie, G. Chen, *Small* **2008**, *4*, 462.

[3] a) Y. Fu, P. Li, L. Bu, T. Wang, Q. Xie, X. Xu, L. Lei, C. Zou, S. Yao, *J. Phys. Chem. C* **2010**, *114*, 1472; b) Y. Fu, P. Li, Q. Xie, X. Xu, L. Lei, C. Chen, C. Zou, W. Deng, S. Yao, *Adv. Funct. Mater.* **2009**, *19*, 1784; c) Y. Fu, C. Zou, L. Bu, Q. Xie, S. Yao, *ACS Appl. Mater. Interfaces* **2013**, *5*, 934.

[4] a) G.-X. Wang, Y. Qian, X.-X. Cao, X.-H. Xia, *Electrochem. Commun.* **2012**, *20*, 1; b) J. Li, G. Cheng, S. Dong, *J. Electroanal. Chem.* **1996**, *416*, 97; c) Q. Zhang, S. Wu, L. Zhang, J. Lu, F. Verproot, Y. Liu, Z. Xing, J. Li, X.-M. Song, *Biosens. Bioelectron.* **2011**, *26*, 2632.

[5] a) J. S. Haghpanah, R. Tu, S. Da Silva, D. Yan, S. Mueller, C. Weder, E. J. Foster, I. Sacui, J. W. Gilman, J. K. Montclare, *Biomacromolecules* **2013**, *14*, 4360; b) H. Liu, J. Song, S. Shang, Z. Song, D. Wang, *ACS Appl. Mater. Interfaces* **2012**, *4*, 2413; c) C. Aimé, T. Coradin, *J. Polym. Sci. Pol. Phys.* **2012**, *50*, 669; d) M. Darder, P. Aranda, M. L. Ferrer, M. C. Gutiérrez, F. del Monte, E. Ruiz-Hitzky, *Adv. Mater.* **2011**, *23*, 5262.

[6] a) A. P. Mathew, M.-P. G. Laborie, K. Oksman, *Biomacromolecules* **2009**, *10*, 1627; b) Y. Huang, X. Qin, Z. Li, Y. Fu, C. Qin, F. Wu, Z. Su, M. Ma, Q. Xie, S. Yao, J. Hu, *Biosens. Bioelectron.* **2012**, *31*, 357; c) X. Lu, Z. Wen, J. Li, *Biomaterials* **2006**, *27*, 5740.

[7] a) C. Qin, C. Chen, Q. Xie, L. Wang, X. He, Y. Huang, Y. Zhou, F. Xie, D. Yang, S. Yao, *Anal. Chim. Acta* **2012**, *720*, 49; b) C. Qin, W. Wang, C. Chen, L. Bu, T. Wang, X. Su, Q. Xie, S. Yao, *Sens. Actuators, B* **2013**, *181*, 375.

[8] a) D. L. Graham, H. A. Ferreira, P. P. Freitas, J. M. S. Cabral, *Biosens. Bioelectron.* **2003**, *18*, 483; b) M. Shim, N. W. Shi Kam, R. J. Chen, Y. Li, H. Dai, *Nano Lett.* **2002**, *2*, 285.

[9] a) O. I. Wilner, Y. Weizmann, R. Gill, O. Lioubashevski, R. Freeman, I. Willner, *Nat. Nanotechnol.* **2009**, *4*, 249; b) O. I. Wilner, S. Shimron, Y. Weizmann, Z.-G. Wang, I. Willner, *Nano Lett.* **2009**, *9*, 2040.

[10] F. Carn, O. Durupthy, B. Fayolle, T. Coradin, G. Mosser, M. Schmutz, J. Maquet, J. Livage, N. Steunou, *Chem. Mater.* **2009**, *22*, 398.

[11] Y. Li, X. S. Sun, *Biomacromolecules* **2010**, *11*, 1847.

[12] a) R. Kita, A. Takahashi, M. Kaibara, K. Kubota, *Biomacromolecules* **2002**, *3*, 1013; b) B. Blombäck, B. Hessel, D. Hogg, L. Therkildsen, *Nature* **1978**, *275*, 501.

[13] a) O. Ziv-Polat, H. Skaat, A. Shahar, S. Margel, *Int. J. Nanomedicine* **2012**, *7*, 1259; b) D. Eyrich, F. Brandl, B. Appel, H. Wiese, G. Maier, M. Wenzel, R. Staudenmaier, A. Goepferich, T. Blunk, *Biomaterials* **2007**, *28*, 55; c) A. Breen, T. O'Brien, A. Pandit, *Tissue Eng. Part B Rev.* **2009**, *15*, 201.

[14] G. Praveen, P. R. Sreerekha, M. Deepthy, V. N. Shantikumar, C. Krishna Prasad, *Nanotechnology* **2012**, *23*, 095102.

[15] a) M. Andersson, J. Andersson, A. Sellborn, M. Berglin, B. Nilsson, H. Elwing, *Biosens. Bioelectron.* **2005**, *21*, 79; b) E. T. O'Brien, M. R. Falvo, D. Millard, B. Eastwood, R. M. Taylor, R. Superfine, *Proc. Natl. Acad. Sci. U.S.A.* **2008**, *105*, 19438; c) L. Müller, S. Sinn, H. Drechsel, C. Ziegler, H.-P. Wendel, H. Northoff, F. K. Gehring, *Anal. Chem.* **2009**, *82*, 658; d) C.-K. Chen, C.-C. Huang, H.-T. Chang, *Biosens. Bioelectron.* **2010**, *25*, 1922.

[16] T. C. Hageman, H. A. Scheraga, *Arch. Biochem. Biophys.* **1974**, *164*, 707.

[17] H. Liu, N. Hu, *Electroanalysis* **2007**, *19*, 884.

[18] J. H. Kim, C. H. Chung, B. H. Chung, *Analyst* **2013**, *138*, 783.

[19] Q. Yang, J. Liang, H. Han, *J. Phys. Chem. B* **2009**, *113*, 10454.

[20] S. Benson, J. M. Seehof, *J. Am. Chem. Soc.* **1951**, *73*, 5053.

[21] J. Sund, H. Alenius, M. Vippola, K. Savolainen, A. Puustinen, *ACS Nano* **2011**, *5*, 4300.

[22] Y. Fu, C. Chen, Q. Xie, X. Xu, C. Zou, Q. Zhou, L. Tan, H. Tang, Y. Zhang, S. Yao, *Anal. Chem.* **2008**, *80*, 5829.

[23] Y. Fu, T. Wang, L. Bu, Q. Xie, P. Li, J. Chen, S. Yao, *Chem. Comm.* **2011**, *47*, 2637.

[24] a) O. A. Raitman, E. Katz, A. F. Bückmann, I. Willner, *J. Am. Chem. Soc.* **2002**, *124*, 6487; b) P.-C. Nien, T.-S. Tung, K.-C. Ho, *Electroanalysis* **2006**, *18*, 1408; c) C. P. McMahon, G. Rocchitta, P. A. Serra, S. M. Kirwan, J. P. Lowry, R. D. O'Neill, *Anal. Chem.* **2006**, *78*, 2352; d) D. Pan, J. Chen, S. Yao, L. Nie, J. Xia, W. Tao, *Sens. Actuators, B* **2005**, *104*, 68.

[25] a) J. Li, X. Lin, *Biosens. Bioelectron.* **2007**, *22*, 2898; b) C. Deng, M. Li, Q. Xie, M. Liu, Q. Yang, C. Xiang, S. Yao, *Sens. Actuators, B* **2007**, *122*, 148.

[26] A. Biswas, I. S. Bayer, H. Zhao, T. Wang, F. Watanabe, A. S. Biris, *Biomacromolecules* **2010**, *11*, 2545.

[27] J. Zhang, S. Song, L. Wang, D. Pan, C. Fan, *Nat. Protocols* **2007**, *2*, 2888.